Aeroacoustics Conferences
20-23 May 2019, Delft, The Netherlands
25th AIAA/CEAS Aeroacoustics Conference

10.2514/6.2019-2603

New modular fan rig for advanced aeroacoustic tests: acoustic characterization of the facility

É. Salze [a], A. Pereira and P. Souchotte
Univ Lyon, École Centrale de Lyon and LMFA UMR CNRS 5509, Écully, France, F-69134

J. Regnard, F. Gea-Aguilera and M. Gruber
Safran Aircraft Engines, Département Aérodynamique et Acoustique, 77550 Moissy Cramayel, France

This paper presents the acoustic qualification of the new ECL-B3 test-rig at École Centrale de Lyon in France. This new experimental facility is part of the PHARE project, which is supported by the French National Research Agency through the EquipEx program. The test-rig was designed and manufactured together by Safran Aircraft Engines and École Centrale de Lyon for aeroacoustic tests of a reduced-scale fan stage, and can support a wide range of R&D studies using state-of-the-art equipment and instrumentation, such as turbulence control screen, pole rakes, hot-wires, particle image velocimetry, pressure transducers, and internal and external microphone arrays, among others. These will allow for a better understanding of aeroacoustic phenomena in future fan stages, such as the influence of inflow distortion, aerodynamic instabilities due to rotating stall and surge, and noise generation and propagation. Furthermore, the high-speed acquisition system that has been set up in the test facility is suitable for highly instrumented aeroacoustic measurements. For instance, up to 192 microphones can be installed simultaneously. Commissioning tests have been performed using a 20'' fan stage designed and manufactured by Safran Aircraft Engines. Preliminary results indicate that this facility can provide state-of-the-art aeroacoustic measurements (low inlet distorsion, low background noise levels, ...), and can be useful for advanced aeroacoustic tests of modular fan stages. Thus, the ECL-B3 facility is suitable for the maturation of noise reduction technologies up to technology readiness level of the order of 3 to 4.

I. Introduction

The coming generation of Ultra High Bypass Ratio (UHBR) turbofan engines is expected to come with an increase in the fan diameter and a reduction of the exhaust jet speed, fan rotation speed and intake length. From an acoustic perspective, the fan stage will be a major source of noise for future UHBR turbofan engines. The reduction of the fan rotation speed shifts the Blade Passing Frequency (BPF) towards lower frequencies compared to the current generation of turbofan engines. Conventional acoustic liners cannot operate at their maximum efficiency on short and thin nacelles and advanced technologies need to be developed and tested. Furthermore, the inflow distortion due to the reduced intake length could potentially increase tonal and broadband noise levels from the fan stage. Therefore, UHBR turbofan engines present several acoustic challenges that need to be addressed to ensure further noise reductions, as set by the Advisory Council for Aeronautics Research in Europe (ACARE) [2].

Engine manufacturers rely on high-fidelity experimental measurements performed in dedicated facilities for engine testing. To this end, a number of aeroengine fan rigs for aeroacoustic measurements in static test conditions are operated around the world [8, 13, 15, 22]. Most of them present some common characteristics. For example, the testing room is usually an anechoic chamber that reproduces free-field conditions and prevents noise reflections from contaminating the acoustic measurements. A far-field microphone array, which is often located at a similar height to that of the fan shaft, is used for noise directivity measurements. All of them use a Turbulence Control Screen (TCS), which is also referred to as Inlet Control Device (ICD), to reduce the inflow distortion at the fan intake and reproduce realistic in-flight conditions [18, 23]. Furthermore, fan rigs usually support in-duct microphone arrays for unsteady wall-pressure measurements and modal decomposition[11, 21]. Additionally, wind tunnel facilities with large test sections have also been used for aeroengine noise tests, which might be useful to assess fan noise from wind-cross,

[a]Corresponding author, edouard.salze@ec-lyon.fr

and angle-of-attack configurations, and innovative aeroengine architectures, such as Counter-Rotating Open Rotors (CROR) [4, 14, 20].

Recently, Safran Aircraft Engines and Ecole Centrale de Lyon designed, manufactured and instrumented together a new test-rig called ECL-B3 for high-quality aeroacoustic measurements of a reduced-scale fan stage. The ECL-B3 facility has been designed to support a wide range of R&D studies using state-of-the-art equipment and instrumentation, such as a TCS, pole rakes, hot-wires, Particle Image Velocimetry (PIV), pressure transducers, and internal and external microphone arrays with a wide dynamic range, among others. These will allow for a better understanding of aeroacoustic phenomena in fan stages, such as inflow distortion, aerodynamic instabilities due to rotating stall and surge [6], and noise generation and propagation[17]. Furthermore, this modular fan rig is suitable for the maturation of noise reduction technologies up to Technology Readiness Level (TRL) of the order of 4, which will help the aerospace industry to meet stringent noise regulations.

This paper is organized as follows. The ECL-B3 test-rig is described in Section II. The quality of far-field measurements is discussed in Section III, including the influence of the far-field microphones set-up, and the qualification of the anechoic chamber. In-duct measurements are described in Section IV, which includes information about the repeatability of noise measurements, the influence of the test-rig configuration such as the presence of the TCS, and a wavenumber analysis to separate the fan noise from other sources.

II. The ECL-B3 test-rig at École Centrale de Lyon

A. Overview of the test-rig

The new ECL-B3 test-rig at École Centrale de Lyon presents three main rooms, as shown in Fig. 2: an anechoic chamber containing the fan stage (see Fig. 1 on the right), a power supply room, and a basement with the Venturi tube and the exhaust circuit. The air intake, which is located on the roof of the anechoic chamber, presents a rectangular passage and contains 2 rows of silencers, which quieten and smoothen the flow before entering the testing room. The air intake also prevents noise from being emitted on the campus at École Centrale de Lyon. The dimensions of the testing room are 5.5 m $\times$ 6 m $\times$ 7 m, approximately. This testing room contains a series of wedges on the walls such that it behaves as an anechoic chamber for frequencies above 200 Hz. A footbridge within the testing room is used to provide full access to the installed testing machine (see Fig. 1 on the left).

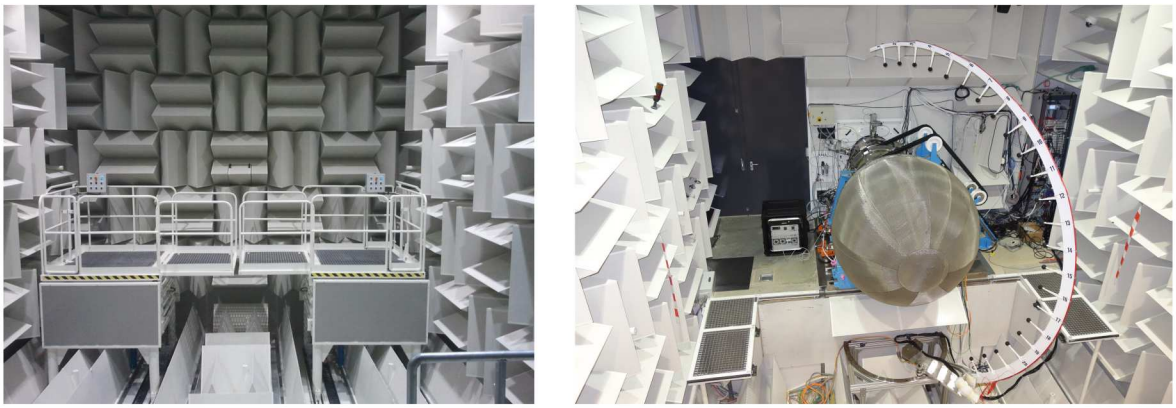

Fig. 1 On the left : anechoic chamber of the test-rig. On the right : TCS and external arc of microphones in the anechoic chamber of the ECL-B3 facility.

The power supply room contains the generator shaft, the torque transmission system towards the fan shaft, and a variable valve system close to the throttle. The power supply system can provide a mechanical power of up to 3 MW to the generator shaft. The variable valve system has been designed to control the massflow rate and the pressure ratio at

a constant fan speed in safe conditions, which is useful for studying aerodynamic instabilities outside the fan operating line [6]. The throttle turns the flow towards a Venturi tube, which is used to measure the massflow rate. Finally, the flow exhausts from a row of silencers, which minimize external noise emissions.

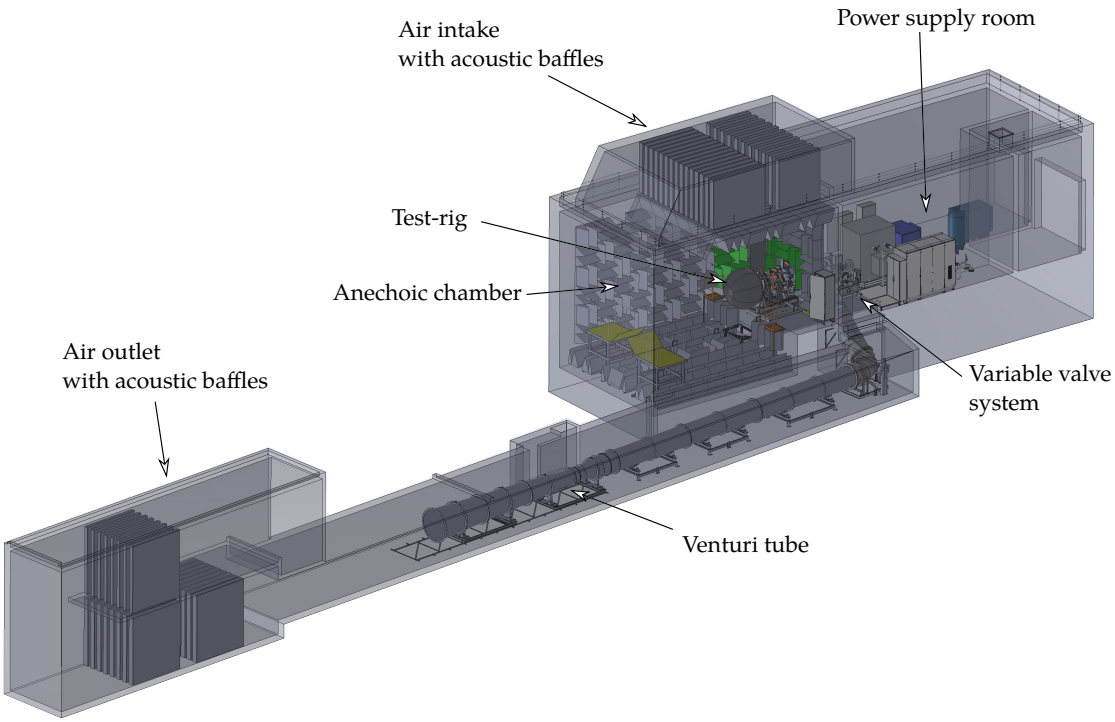

Fig. 2 Schematic representation of the ECL-B3 facility.

A comparison of available data from various fan rigs and facilities is shown in Table 1, including the ECL-B3 facility at École Central de Lyon, the C-3A facility at the Central Institute of Aviation Motors (CIAM) [13, 18], and the fan rig of AneCom AeroTest (ACAT) [15].

	ECL-B3	C-3A (CIAM) [13, 18]	ACAT [15]
fan diameter, D_{Fan} [m]	0.508	0.7	1.14
maximum shaft speed [rpm]	16 000	13 000 (2 shafts)	12 000
maximum mass flow rate [kg/s]	45	67	200
maximum shaft power [MW]	3	2.5 (each shaft)	18
far-field distance [m]	2	4 - 5	18.5
room dimensions [m^3]	$5.5 \times 7 \times 6$	$14.5 \times 15.5 \times 5$	$30 \times 35 \times 10$
TCS diameter [m]	2	2.03	2.78

Table 1 Characteristics of various aeroengine fan rigs.

B. Acoustic instrumentation

Upstream noise directivity is measured using an array of 27 G.R.A.S. 46BE-S4 1/4" free-field microphones, installed with a windscreen. The microphones are positioned over a portion of a 2m semi-circle from the fan intake, as shown in Fig. 3. Microphones are uniformly distributed over a circular array ranging from $\Phi = -76.2^o$ to 103.8^o (see Fig.1 on the right). Furthermore, the array of microphones can be rotated between -84° and 73° to fully characterize the upstream noise propagation over a half sphere.

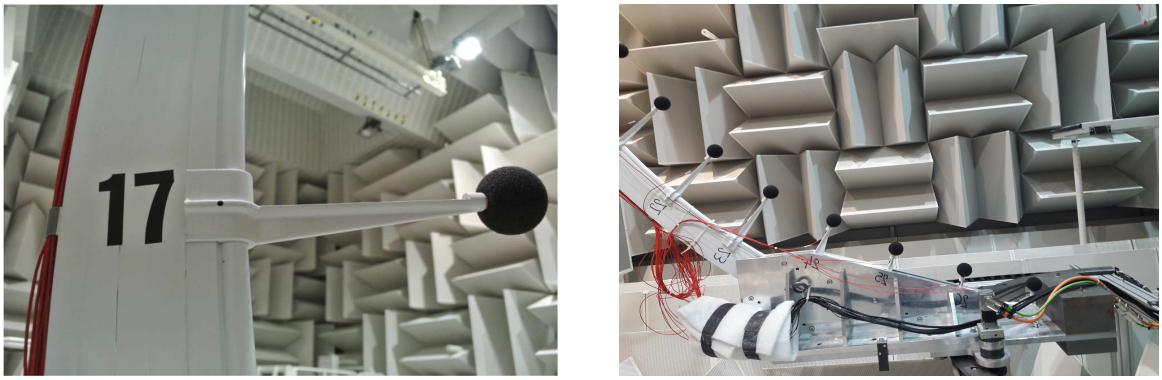

Fig. 3 On the left: microphone support with the windscreen. On the right: rotating system of the external directivity array.

The location of the external arc of microphones meets the ISO3745:2012 standards [12] for anechoic chambers. The compliance with the ISO3745:2012 standards was assessed by measuring the noise attenuation from a monopole source (placed at the fan intake position without the fan rig) to the observer location between 100 Hz and 20 kHz. The far-field characteristics of the external arc of microphones are given in Table 2, where the observer distance is set to $d = 2$ m from the fan intake, λ represents the acoustic wavelength, and the Fraunhofer distance is given by $2D_{fan}^2/\lambda$. Additionally, 4 fixed reference microphones have been placed near the 4 corners of the ceiling in the testing room.

d/D_{Fan}	d/λ	$2D_{fan}^2/\lambda$
4	2.3 at 400 Hz, 233 at 40 kHz	3.3 at 400 Hz, 0.033 at 40 kHz

Table 2 Far-field characteristics of the external arc of microphones.

The 20” UHBR fan stage has been designed to accommodate up to 160 in-duct 1/4" G.R.A.S. 46BG or 47BX-S6 flush-mounted microphones at different internal locations depending on the fan rig configuration. Kulite pressure transducers can also be installed for unsteady wall pressure measurements. The microphones have been modified by the manufacturer to ensure their robustness in extreme conditions, such as surge, stall and instabilities in the fan stage. The locations of these sensors have been optimized for advanced aero-acoustic measurements, such as circumferential and axial modal decomposition [10, 16, 17]. It is also important to emphasize that several in-duct microphones are positioned onto rotating rigs (up to 4 in total), which allows in-duct pressure measurements on a large number of locations with minimal instrumentation. The schematic representation of the acoustic instrumentation is shown on Fig. 4.

In this paper, only acoustic measurements from 3 control microphones and an axial microphone array are presented to assess the quality of in-duct acoustic measurements in Section IV. A schematic representation of the internal acoustic instrumentation that is used for the commissioning of in-duct acoustic measurements is presented in Fig. 4. The 3 control microphones are located at approximately 0.25 D_{Fan} upstream of the fan leading edge (microphone M_A),

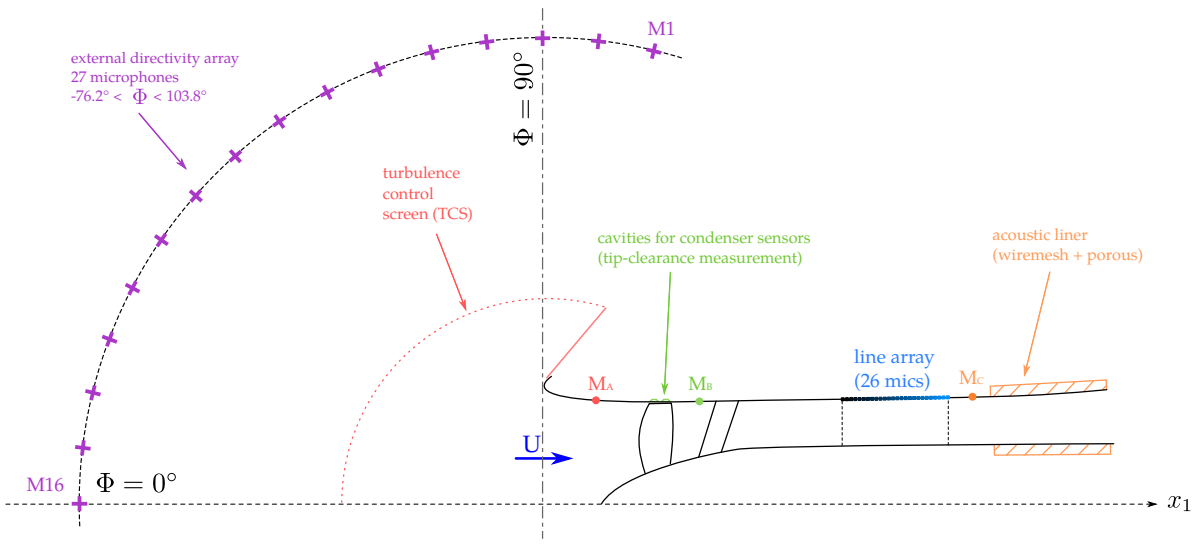

Fig. 4 Acoustic instrumentation used for the commissioning of the facility: M_A, M_B and M_C used to analyzed the effects of the TCS, of the clearance cavities, and of the acoustic treatment, respectively. The downstream line array contains 26 microphones. The upstream far-field array contains 27 microphones.

0.05 D_{Fan} downstream of the fan trailing edge in the interstage (microphone M_B), and 1.5 D_{Fan} downstream of the OGV trailing edge (microphones M_C). The axial microphone array contains 26 uniformly distributed microphones. The axial separation between 2 neighboring microphones was set to 11 mm. The first microphone of the line array was placed at 0.8 D_{Fan} downstream of the OGV trailing edge. This microphone array is suitable for the axial wavenumber decomposition and therefore, it can be used to separate the hydrodynamic contribution of the boundary layer from upstream- and downstream-propagating acoustic waves in the duct.

All signals are simultaneously sampled at 102 kHz over 24 bits, using a National Instrument front-end set-up. The acquisition rate was chosen to cover the bandwidth of interest after scaling the UHBR fan stage up to full size. The set-up contains NI-4499 high-frequency acquisition cards, and allows data acquisition up to 192 channels. In-house monitoring, measurement and post-processing systems have been designed and coded by the authors using LabView.

III. Assessment of far-field measurements

A. Qualification of the microphone set-up

Each microphone is set on an arch structure using a dedicated support, as shown in Fig. 4. The installation effect of such a microphone set-up was checked using an electrical spark source. The spark source is made of two tungsten electrodes, separated by a gap of 1 cm, connected to an electrical potential of 20 kV. The sudden heating, initiated by the spark, generates a spherical pressure wave with a high amplitude (about 500 Pa at a distance of 30 cm from the source) and a short duration (about 50 μs). The directivity of the source has been investigated in a previous study [19].

The spark source was positioned in the test-rig at the center of the inlet. The pressure wave propagates towards the far-field microphones. First, the time of of arrival t_0 of the direct wave was used to fine-tune the source - microphone distance, with an accuracy better than 2 mm. The other wavefronts were used to identify the different contributions from diffracting objects in the testing room, as shown in Fig. 5. Two contributions can be clearly identified. The first contribution is due to the diffraction produced by the support end (1), where the amplitude is 32 dB below the direct pressure wave. The second contribution is due to the diffraction produced by the array support (2), where the amplitude is 35 dB below the direct pressure wave. The amplitude of the diffracted pressure wave is found small enough to garantee accurate far-field acoustic measurements.

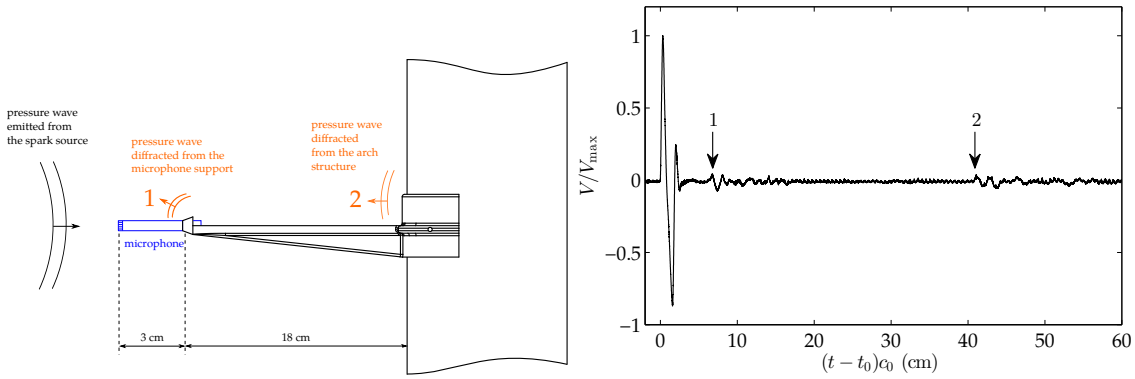

Fig. 5 On the left : schematic representation of the microphone support with two contributions identified. On the right : output voltage V of the microphone. The x-axis is transformed into distance using a retarded time.

B. Qualification of the anechoic room

Most walls and surfaces of the anechoic room were treated using acoustic wedges, as shown in Fig. 1. Nevertheless, some parts of the anechoic chamber were not acoustically treated to allow for the installation of the test vehicule, such as the concrete floor, and other parts were treated with acoustic foam panels without wedges, such as the walls around the variable valve system. Before the installation of the test vehicule, an acoustic characterization of the anechoic room was performed. The anechoic room is shown in Fig. 6 in correct proportions, where the following reflections can be identified : on the concrete floor (E1), on the variable valve system exhaust (E2), on the acoustic panels (E3 and E4). Minor reflections have also been identified, on the variable valve exhaust (E12 and E13, see Fig. 6). The corresponding time delays between the direct wave and the reflected waves were calculated using the method of image sources, as shown in Fig. 6.

The times of arrival of the different waves were measured using the spark source positionned at the center of the circular array. The resulting map of impulse responses is plotted in Fig. 7, where Φ denotes the angle on the circular array, $\Phi = 0°$ being the horizontal axis, t_0 is the time of arrival of the direct wave, and c_0 is the speed of sound. The amplitudes of the reflected waves were normalized by the amplitude of the direct wave emitted by the spark source to assess the acoustic attenuation. Several reflections are observed. The reflection from the concrete floor (E1) is visible on the upper part of the antenna. The associated attenuation is around -25 dB. Reflections on the side wall (E2, E3), treated using foam panels, are also visible, with an attenuation of around -15 dB. The reflection from the ceiling (E4) is not visible.

It can be concluded that the amplitudes of the reflected waves are significantly below the amplitude of the direct wave. Therefore, the upstream directivity array can provide accurate results from acoustic measurements of the fan stage.

IV. Assessment of in-duct acoustic measurements in the test vehicule

A. Methodology and signal processing

In this section, the quality of in-duct acoustic measurements is assessed at various internal locations. Pressure spectra and cross-spectra between microphones are estimated from time series using the Welch method,

$$S(\boldsymbol{\xi}, f) = \frac{2\pi}{T}\frac{1}{N}\sum_{n=1}^{N}\hat{p}_n(\boldsymbol{x}_0, f)\hat{p}_n^{\star}(\boldsymbol{x}_0 + \boldsymbol{\xi}, f) \tag{1}$$

where $\boldsymbol{\xi}$ is the separation vector between two microphones, T is the length of a signal bloc, N is the total number of averages, and $.^{\star}$ represents the conjugate of a complex quantity. In practice, the wall-pressure field is assumed to exhibit homogeneous statistical properties over the line array, such that $S_{ij}(\boldsymbol{x}, \boldsymbol{\xi}, \omega) = S_{ij}(\boldsymbol{\xi}, \omega)$. The one-dimensional

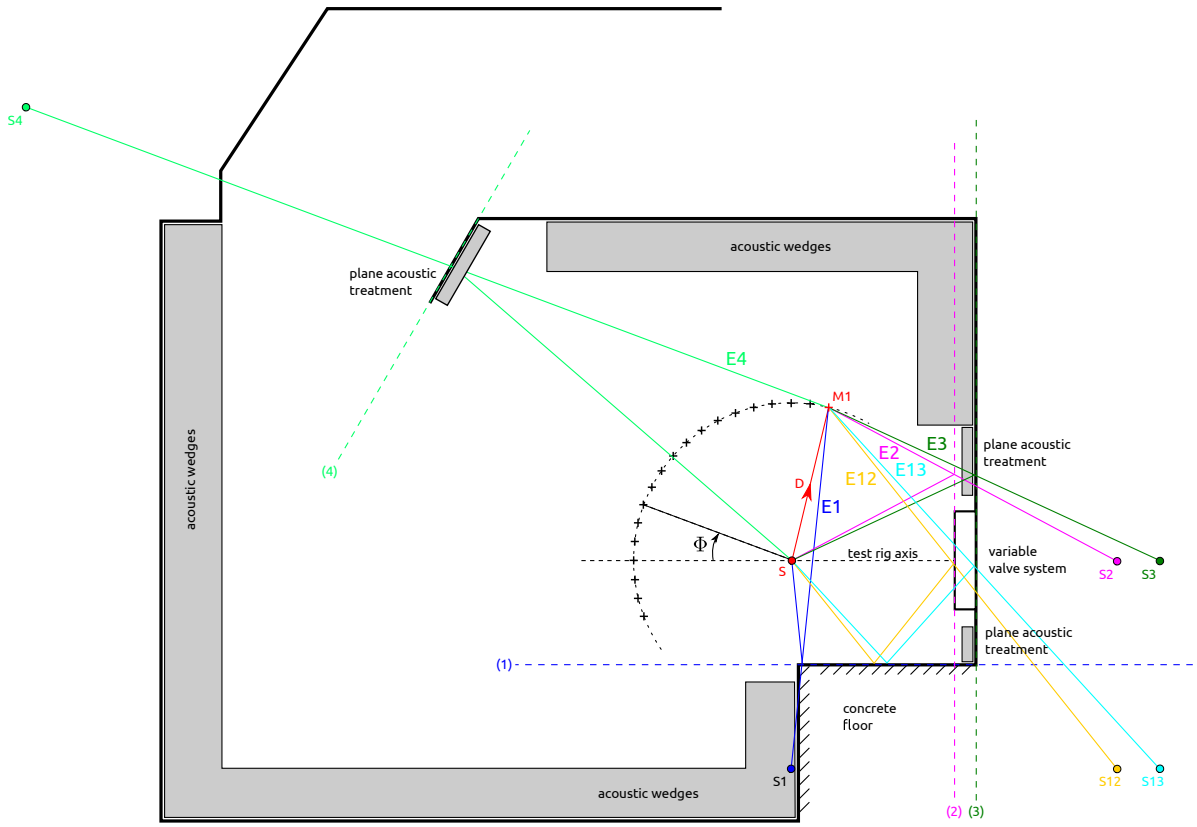

Fig. 6 Plan of the anechoic room in the correct proportions, before the installation of the fan stage. An electric spark source S is placed at the center of the upstream microphone array. Potential reflections can be identified *a priori*.

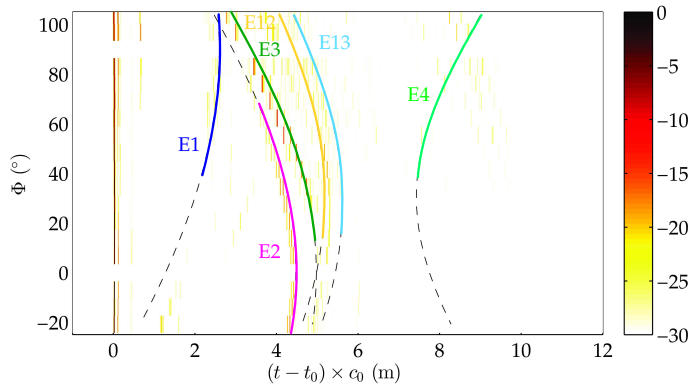

Fig. 7 Impulse response map from the microphones of the upstream array. Amplitudes in dB, normalized by the amplitude of the direct wave.

streamwise wavenumber-frequency spectrum is directly computed by discretizing the following Fourier integral

$$\Phi_{pp}(k_1, \omega) = \frac{1}{2\pi} \int S_{ij}(\xi_1, \omega) e^{-ik_1\xi_1} d\xi_1 \tag{2}$$

where k_1 is the streamwise wavenumber. In the absence of flow, the wavenumber spectrum is characterized by contributions inside the acoustic disk of radius $k_0 = \omega/c_0$. In the presence of flow, a second contribution, due to the convection of wall-bounded turbulence, is located at $k_c = \omega/U_c$ [1, 5, 7, 9]. This second contribution is sometimes called the "boundary layer noise" in the literature. The interest of such a representation of the wall-pressure field is that

it provides an explicit separation between the acoustic and the hydrodynamic pressure fields. The acoustic spectrum can be recovered from the wavenumber representation obtained through Eq. 2 by integrating the acoustic wavenumbers as

$$S_{\mathrm{ii}}(\omega) = \int_{-k_0}^{+k_0} \Phi_{pp}(k_1, \omega) \mathrm{d}k_1 \tag{3}$$

The method described in Eq. 3 can be applied to recover the downstream propagating acoustic waves by integrating the positive wavenumbers or the upstream propagating field by integrating the negative wavenumbers. It should be noted that the convection of acoustic waves by the mean flow has to be included in the dispersion relation for an accurate definition of the acoustic region.

A preliminary measurement has been performed without flow. A Bruel and Kjaer type 4295 source is placed in the inlet at $x_1 = 0$. The resulting one-dimensionnal wavenumber spectrum is plotted at the top of Fig. 8. The acoustic wavenumbers resulting from duct modes are clearly visible. It can be noted that the positive wavenumbers exhibit larger amplitudes than the negative ones. This behavior is due to the presence of the downstream acoustic liner which attenuates waves from the rear part of the machine (from the right to the left on Fig. 4).

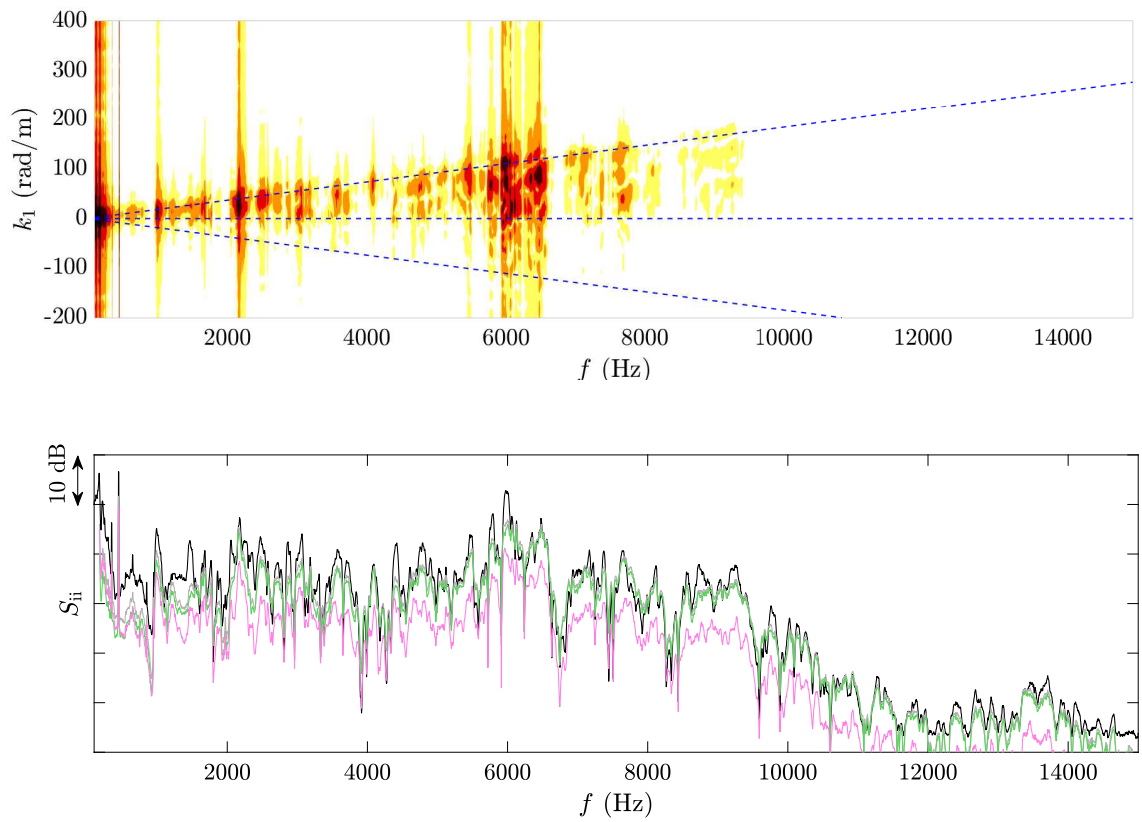

Fig. 8 Above : one-dimensional wavenumber spectrum of the pressure, obtained downstream of the fan stage through Eq. 2, using an acoustic source located in the inlet at $x_1 = 0$. Below : —— : Wall-pressure spectrum, —— : acoustic spectrum (integrated over the acoustic wavenumbers),
—— upstream propagating waves, —— downstream propagating waves.

The resulting acoustic spectra from Fig. 8 have been computed for various wavenumber integration limits at the bottom of Fig. 8. Overall, the acoustic spectrum from upstream-propagating waves is around 5 dB lower than that of the downstream propagating waves. Thus, spurious reflections coming from the rear part of the machine are expected to be significantly lower than fan noise. This assumtion is verified in Section IV.E.

B. Background noise

Background noise is measured in two configurations, and compared to fan noise at approach conditions. The first configuration is obtained with all the supply systems switched off. The second configuration is obtained with the air and oil supply systems turned on, and represents the *real* background noise during the acoustic measurements. Compared to the first configuration, the oil and air supply systems exhibit a contribution of about 10 to 20 dB, as can be seen on Fig. 9. During the test campaign, fan noise at approach condition is 40 dB higher than the background noise, for all the considered bandwidth.

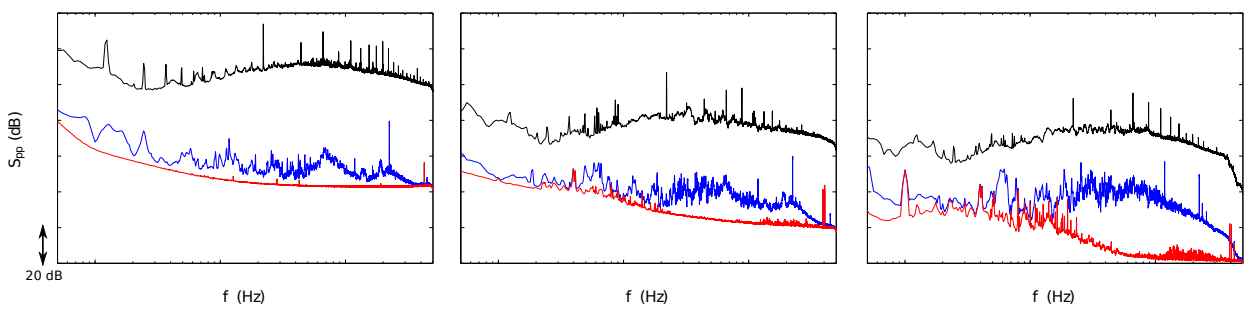

Fig. 9 Background noise of the test-rig, compared to measurements during the test campaign. On the left : internal measurement (microphone M_A) ; center : microphone from the far-field directivity array ; on the right : external reference microphone in the anechoic chamber. —— : Fan noise at approach ; —— : Background noise with air and oil supply systems ; —— : Facility background noise.

C. Statistical convergence of spectal quantities

The statistical convergence of spectral quantities was found to reduce as $1/\sqrt{N}$ for the auto-spectra, and as $1/\sqrt{\gamma N}$ for cross-spectra, where γ is the coherence between two pressure signals [3]. In other words, the statistical convergence is improved when a large number of averages is used. Additionally, a lower coherence leads to a slower convergence of the cross-spectra. The statistical convergence can be improved by increasing the number of averages. This can be obtained by acquiring longer signals, or by windowing shorter time periods T. These solutions are however not convenient for turbomachinery testings. Acquiring longer signals makes the test campaign last longer and be more expensive. In the Welch process, windowing shorter time periods leads to a worse frequency resolution of the spectral quantities, which is not desirable for the analysis of spectra with tonal noise such as blade passing frequencies. For instance, if a 1 min signal is acquired and post-processed using time periods of $T = 250$ ms, the Welch method gives a frequency resolution of $\Delta f = 4$ Hz and a number of $N = 240$ averages. The statistical error is around 6% on the spectra estimation, and around 20% on the cross-spectra estimation. The acquisition time is therefore an important parameter to be adjusted.

During the first test campaign, a 20 min recording has been performed to estimate the statistical convergence in experimental conditions. The time series are used to compute spectra in the inlet. Cross-spectra are estimated between two microphones at the same axial position in the inlet, at opposite angular locations. The time period T is fixed at 250 ms. Integrated pressure levels are computed over various time length from the spectra and cross-spectra as described in Eq. 1. The frequency bandwidth of interest are the first and second blade passing frequencies, and the whole bandwidth. The difference between the level obtained after the 20 min of acquisition, and the level obtained after a shorter time period, is plotted in Fig. 10 for the auto-spectrum. Considering a threshold of ±0.1 dB, the experiment yields an acquisition time of about 1 min for the auto-spectrum estimation. The same procedure is applied for the cross-spectrum, reported in Fig. 11. The cross-spectra, whose convergence is slower, should be estimated over signals of at least 8 min, considering the same criterion and the same averaging parameters.

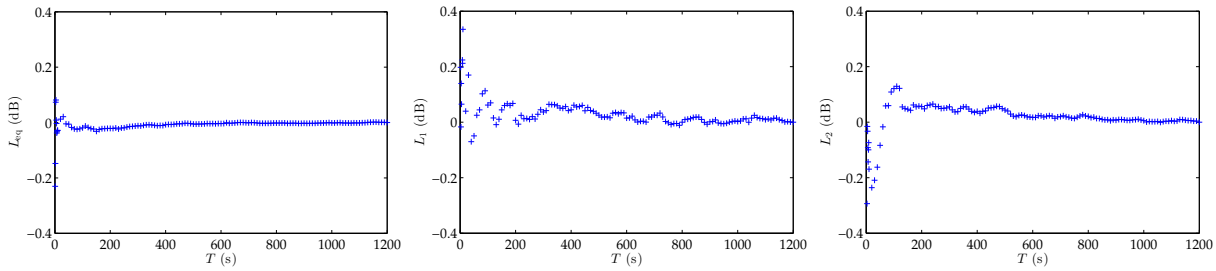

Fig. 10 Convergence of the auto-spectra (microphone M_A). On the left : overall pressure level ; center : first blade passing frequency ; on the right ; second blade passing frequency. Difference (in dB) between a 20 min acquisition, and a shorter acquisition.

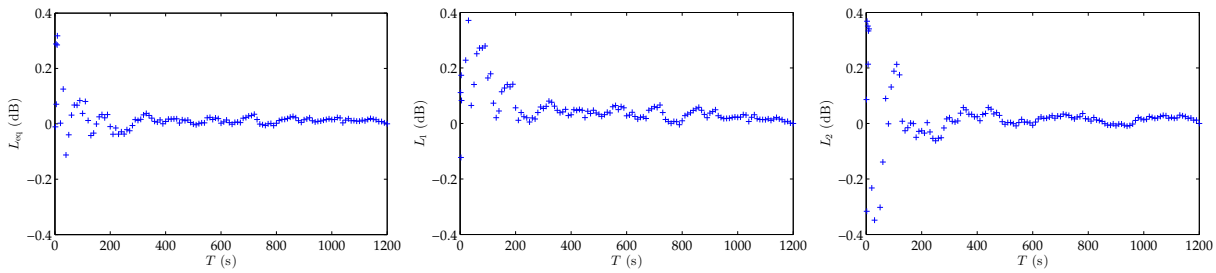

Fig. 11 Convergence of the cross-spectra (between microphone M_A and another microphone at the same axial location in the inlet, not represented in Fig. 4). On the left : overall amplitude ; center : first blade passing frequency ; on the right ; second blade passing frequency. Difference (in dB) between a 20 min acquisition, and a shorter acquisition.

D. Repeatability of noise measurements

During the first test campaign in the ECL-B3 test-rig, noise measurements have been performed 35 times on different days, at the same operating point. Differences of less than 0.5% and 0.1% have been observed in the mean mass flow rate and in the pressure rise of the fan stage, respectively. A 2 min recording of the pressure signals has been performed at each stabilized operating point, and the resulting pressure spectra were computed and compared (see Fig. 12 on the left). Very small variations can be observed, which are mainly found on the peaks amplitudes. The integration of spectral amplitudes shows fluctuations of less than 0.3 dB on the overall level (i.e. integrated over the whole bandwidth). Integrated levels over smaller bands around the first to fifth blade passing frequencies show larger fluctuations, of the order of ±2 dB.

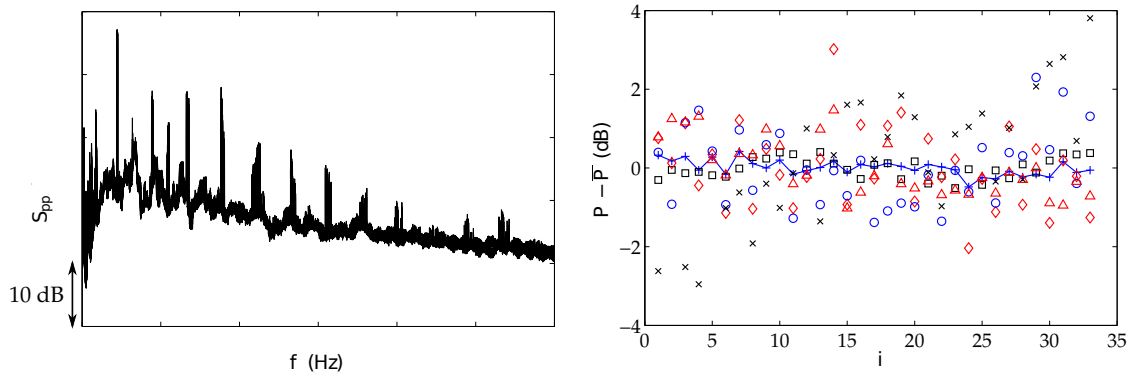

Fig. 12 Repetability of external noise measurements. On the left : 35 pressure spectra estimated at different days for the same operating point. On the right : level variations : —— : absolute level ; □, ◇, ○, × and △ : levels around the first, second, third, fourth and fifth BPF, respectively.

E. Impacts of test-rig setup

The impact of several test-rig configurations on the acoustic results is analyzed in this section. For the same operating point at approach conditions, it was possible to observe the influence of the TCS, the influence of cavities for tip clearance measurements, and the effect of the downstream acoustic liner (see Fig. 4). The TCS is a 2 m diameter sphere, centered at the fan intake, made of layers of wiremesh and honeycomb panels. The impact of the TCS has been measured by the internal microphone M_A (see Fig. 4) at the same operating point of the test-rig. The resulting spectra are plotted in Fig. 13, where the frequency axis is normalized by the blade passing frequency of the rotor f_0. It can be noted that, at the considered operating point, the broadband contribution in the spectrum remains unchanged, within less than 0.2 dB, which corresponds to the repetability confidence of the test-rig. However, the analysis at higher rotational speeds (not reported in this paper) revealed a broadband reduction of at least 4 dB if the TCS is used. A large reduction of the broadband noise has also been observed on the far-field spectra, but not reported in this paper.

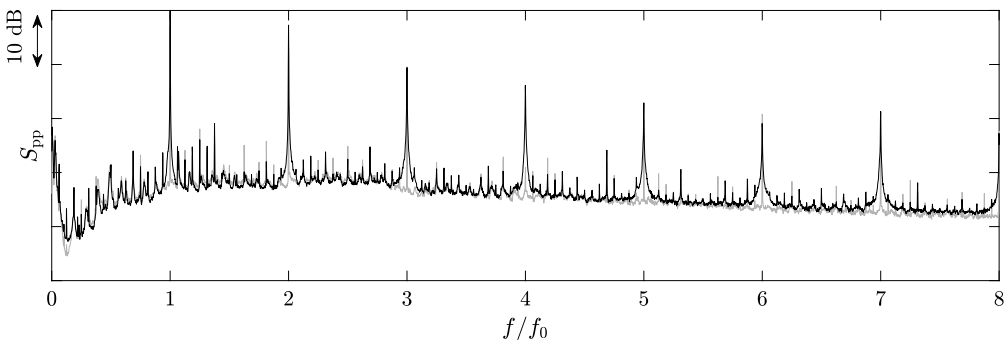

Fig. 13 Impact of the TCS. —— : without TCS, —— : with TCS. Measurement performed in the inlet by microphone M_A (see Fig. 4).

The tonal components, resulting from the rotation of the stage, exhibit some differences. Without the TCS, the peaks are notably wider than with TCS, which is consistent with previous work [18, 23]. For instance, at the first blade passing frequency $f = f_0$, the tone is approximately 16 Hz wide with the TCS, whereas it is about 200 Hz without it. This widening of the tones at the harmonics of the blade passing frequencies can be explained by the ingestion of an unsteady flow distortion, which alters the periodicity of the rotor interactions.

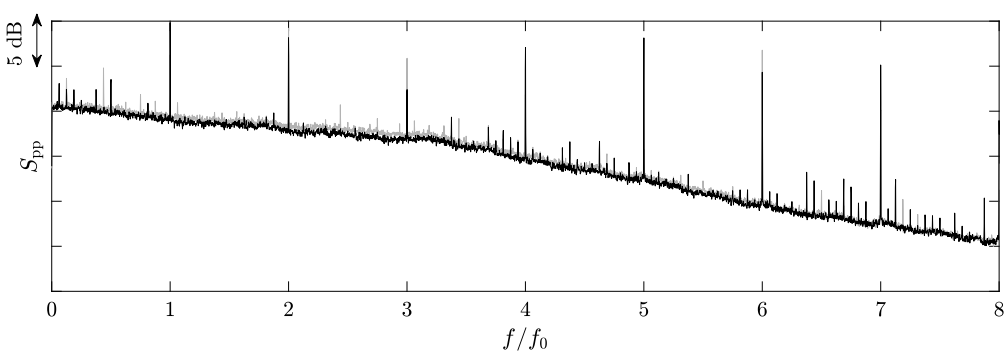

Fig. 14 Impact of clearance cavities. —— : cavities opened, —— : cavities sealed. Measurement performed in the interstage by microphone M_B (see Fig. 4).

Another control measurement has been performed to assess the effect of cavities in the fan tip clearance. These cavities are used to host condenser sensors that are needed for clearance measurements. During acoustic measurements, these cavities are normally sealed to obtain a better representativity of the fan stage sources. Their dimensions are about 1 cm in diameter and 3 mm in depth. The effect of these cavities has been measured by microphone M_B in the interstage. The resulting spectra are plotted in Fig. 14, where the spectrum with closed cavities is plotted in grey, and the spectrum with opened cavities is plotted in black. The effect of the cavities is mainly to alter the tonal components

between the blade passing frequencies. If the cavities are sealed, the source of tonal noise is the slight dissymetry of the fan blades, inducing a periodicity and harmonics of the stage passing frequency. If the cavities are opened, each cavity induces an additional interaction at the stage passing frequency, which alters the tonal components between the blade passing frequencies. The same behavior can be observed in the inlet (microphone M_A), not shown here.

The last control measurement was performed to assess the behavior of the acoustic liner located downstream of the line array (see Fig. 4). This liner is intended to attenuate upstream propagating waves, from reflections on the right end of the duct. The spectra of microphone M_C are plotted in Fig. 15, where the grey spectrum has been measured with treatment, and the black one, without treatment. The effect of the treatment is an attenuation of the broadband contribution of the spectrum for frequencies above $f/f_0 = 0.5$ approximately, at approach conditions.

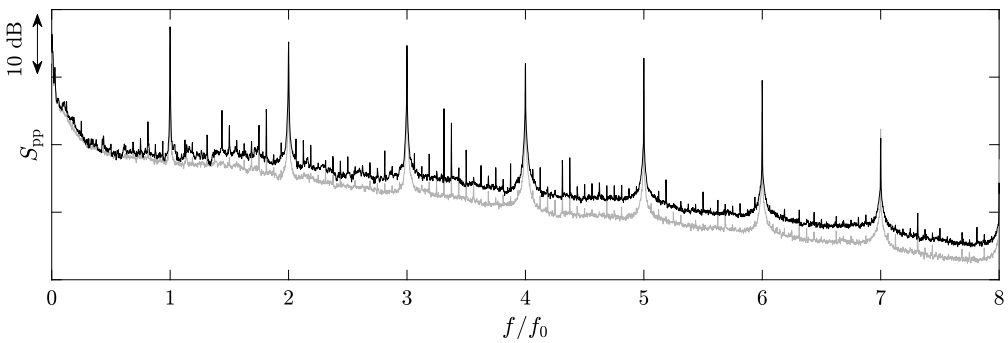

Fig. 15 Impact of downstream acoustic treatment. —— : without treatment, —— : with treatment. Measurement performed downstream of the fan stage by microphone M_C (see Fig. 4).

Additionally, a wavenumber analysis has been performed using the line array. The method is described in Section IV.A. The wavenumber spectrum, obtained through Eq. 2 at the same operating point as in Figs. 13, 14 and 15, is plotted in Fig. 16. One can notice two contributions : the first contribution, located around the convective wavenumber k_c, and the other located inside the acoustic region. The limits are indicated as dashed lines in Fig. 16. The acoustic contribution, obtained through Eq. 3, exhibits larger amplitudes for positive wavenumbers. The upstream propagating waves from reflections on the rigth-end of the duct have been attenuated by the liner shown in Fig. 4.

The integrated spectra from the wavenumber decomposition are compared in Fig. 16 to the one-point frequency spectrum of the first microphone of the line array (see Fig. 4). Firstly, it can be observed that the acoustic spectrum is dominated by the downstream propagating waves, which is consistent with the wavenumber representation. Secondly, the integration of the acoustic spectrum reveals humps and hollows associated to the frequency cut-off of the duct modes for $f/f_0 < 1$ approximately. The contribution from upstream propagating waves is found between 5 and 10 dB below the total acoustic spectrum for f/f_0 between 0.5 and 6, approximately. If f/f_0 is below 0.5, the spectral resolution of the line array does not allow for the separation of different contributions in the wavenumber domain. In comparison with the one-point frequency spectrum of microphone M_1, the acoustic spectrum is of the order of 15 dB below. This difference is due to the contribution of the wall-bounded turbulence, which is convected by the mean flow. This hydrodynamic contribution is found to dominate the wall-pressure signatures at all frequencies of the spectrum, except at the blade passing frequencies where the acoustic contribution dominates. Finally, it should be noted that the integration over the whole wavenumber domain cannot be compared to the one-point frequency spectrum, because the smallest spatial seperations between two neighboring sensors does not allow for the measurement of high-enough wavenumbers. This analysis will be the subject of further studies.

V. Conclusion

A new modular test-rig has been designed and built together by Safran Aircraft Engines and École Centrale de Lyon to improve current understanding of noise sources from a reduced-scaled fan stage This facility has been designed for aeroacoustic measurements that can help to further reduce fan noise from future turbofan engines. To this end, the test-rig has been massively instrumented for advanced in-duct and far-field acoustic analysis, such as modal decomposition and directivity. Additionally, the test bench offers the possibility to include acoustic liners that are representative of

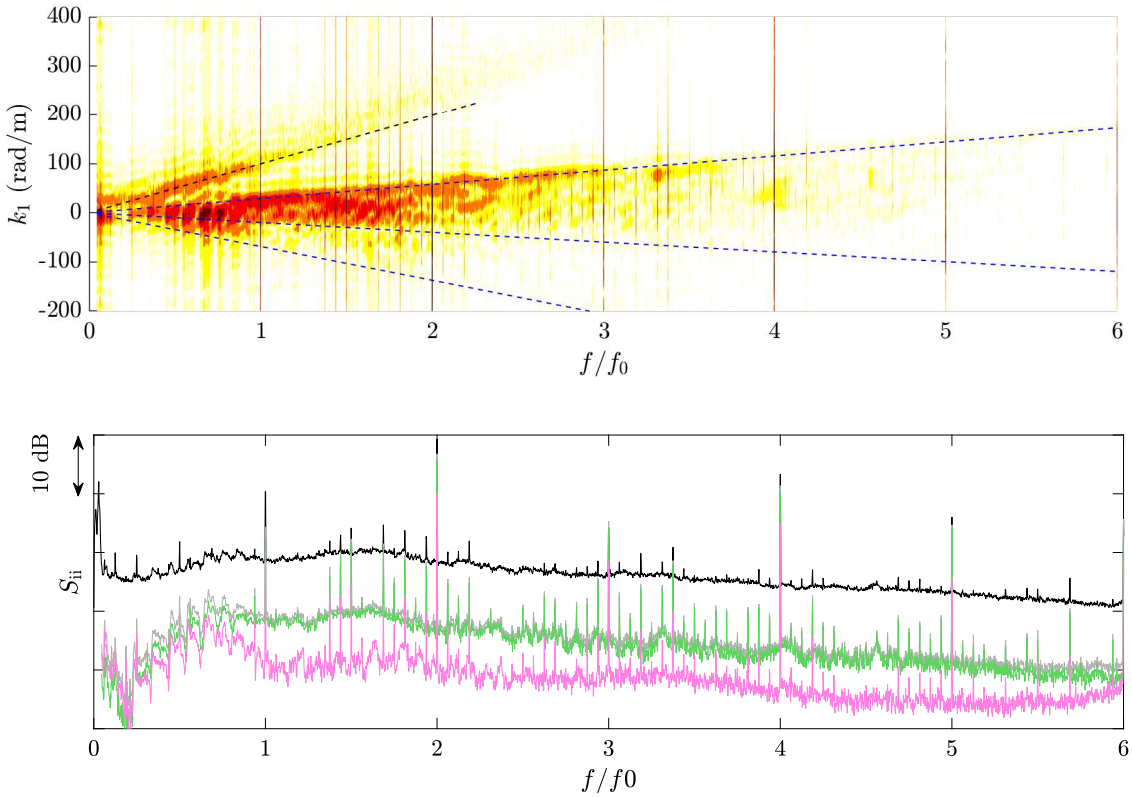

Fig. 16 Above : one-dimensional wavenumber spectrum of the pressure, obtained downstream of the fan stage through Eq. 2. Below : ▬ : Wall-pressure spectrum, ▬ : acoustic spectrum (integrated over the acoustic wavenumbers), ▬ upstream propagating waves, ▬ downstream propagating waves.

full size engines.

A qualification of the far-field microphone set-up and of the anechoic chamber has been performed using an electrical spark source. It was found that diffracted waves originating from the microphone set-up was at least 32 dB below the direct pressure waves, and the reflected waves in the anechoic chamber were found to be at least 15 dB below the direct pressure waves. Thus, it can be concluded that the free-field microphone array can provide accurate results for noise directivity measurements from a fan stage. The quality of internal measurements was examined in different test conditions. The use of a TCS enables a fine description of tonal noise by reducing the ingested distortion and the broadband noise upstream of the fan. The existence of tip-clearance cavities, for the sensors to be mounted, alters the periodicity of the rotor and the structure of tones at the rotor harmonics. If the acoustic liner is installed downstream of the fan stage, the wavenumber decomposition of the in-duct pressure field highlights a difference of 5 to 10 dB between the upstream and downstream-propagating waves, depending on the frequency.

These results indicate that this new modular facility can provide state-of-the-art aeroacoustic measurements, and can be useful for advanced aeroacoustic tests of future fan stages. The ECL-B3 facility is now suitable for the maturation of noise reduction technologies up to technology readiness level of the order of 3 to 4.

Acknowledgments

The present work was financially supported by the French National Research Agency ANR, through the EquipEx program (Plate-formes macHines tournantes pour la mAitrise des Risques Environnementaux, project PHARE 10-EQPX-0043). Financial support from the European Union Seventh Framework Programme (FP7), through the ENOVAL (ENgine mOdule VALidator) project under grant agreement number 604999, is also acknowledged. This work was

performed within the framework of the Labex CeLyA of the Université de Lyon, within the programme "Investissements d'Avenir" (ANR-10-LABX-0060/ANR-16-IDEX-0005) operated by the French National Research Agency (ANR)

The authors would like to express their gratitude for the continous collaboration with Safran Aircraft Engines, whose teams designed and manufactured the fan stage, and provided financal support since the beginning of the PHARE-2 project. The authors would also like to thank Benoît Paoletti, Gilbert Halter and Lionel Pierrard for operating the test-rig and making this research possible. Additionally, the authors would also like to thank Arthur Finez from MicrodB for his help in designing the microphone arrays. Fruitfull discussions with Michel Roger on data post-processing are also acknowledged in the completion of this work.

References

[1] Abraham, B. M. & Keith W. L., 1998, Direct measurements of turbulent boundary layer wall pressure wavenumber-frequency spectra, *J. Fluid Eng.*, **120**, 29-39.

[2] European Commission, Report of the High Level Group on Aviation, Flightpath 2050 Europe's Vision for Aviation, 2011.

[3] Bendat, J. & Piersol, A., 2010, *Statistical errors in basic estimates*, chapter 8 in *Random data, analysis and measurement procedures, fourth edition*, pp 249-285. John Wiley & Sons (Ed.), ISBN 978-0-470-24877-5.

[4] Bergmann, A., 2012, The Aeroacoustic Wind Tunnel DNW-NWB, *18th AIAA/CEAS Aeroacoustics Conference*, No. 2012-2173.

[5] Blake, W.K., 1986, Essentials of turbulent wall-pressure fluctuations, in Mechanics of flow-induced sound and vibration, Vol. II Complex flow-structure interactions, *Academic Press Inc.*, Orlando, Florida.

[6] Brandstetter, C, Paoletti, B. & Ottavy, X., 2019, Compressible modal instability onset in an aerodynamically mistuned transonic fan, *ASME, J. of Turbomachinery*, **141**(3), doi:10.1115/1.4042310.

[7] Bull, M.K., 1996, Wall-pressure fluctuations beneath turbulent boundary layers: some reflections on forty years of research, *J. Sound Vib.*, **190**(3), 299–315.

[8] Cooper, B. A., 1994, A large hemi-anechoic enclosure for community-compatible aeroacoustic testing of aircraft propulsion systems, *Noise Control Engineering Journal*, **42**(1).

[9] Corcos, G. M., 1964, The structure of the turbulent pressure field in boundary-layer flows, *J. Fluid Mech.*, **18**(3), 353–378.

[10] Finez, A., Pereira, A., & Leclere, Q., 2015, Broadband mode decomposition of ducted fan noise using cross-spectral matrix denoising, FAN2015 Conference, 15-17 April 2015, Lyon, France.

[11] Heidelberg, L. J., Hall, D. G., Bridges, J. E. & Nallasamy, M., 1996, A Unique Ducted Fan Test Bed for Active Noise Control and Aeroacoustics Research, *2nd AIAA/CEAS Aeroacoustics Conference*, No. 1996-1740.

[12] *International Organization for Standardization* 2012, Determination of sound power levels and sound energy levels of noise sources using sound pressure - Precision methods for anechoic rooms and hemi-anechoic rooms, ISO 3745:2012.

[13] Khaletskiy, Y., Mileshin, V. & Shipov, R., 2008, Acoustic Test Facility for Aero Engine Fans, *Acoustics'08 Paris*, 1835-1838.

[14] Méry, F., Rey, M., Davy, R. & Fernando, R., 2012, Far field wall-mounted microphone device for the S1MA anechoic closed-section wind tunnel applied to Open Rotor, *18th AIAA/CEAS Aeroacoustics Conference*, No. 2012-2228.

[15] Mueller, D., Schulz, H.-J., Zitouni, G. & Baumann, W., 2005, Europe's Largest Aero Acoustic Test Facility for Aero Engine Fans - The Development and Operation of the AneCom AeroTest Anechoic Chamber, *11th AIAA/CEAS Aeroacoustics Conference*, No. 2005-3050.

[16] Pereira, A., Finez, A., Leclère, Q., Salze, E. & Souchotte, P., 2016, Modal identification of a small-scale ducted fan, *8th AIAA/CEAS Aeroacoustics Conference*, 2016-3063.

[17] Pereira, A., Salze, E., Regnard, J., Gea-Aguilera, F., Gruber, M., 2019, New Modular Fan Rig for Advanced Aeroacoustic Tests - Modal decomposition on a 20" UHBR fan stage, *25th AIAA/CEAS Aeroacoustics Conference*.

[18] Pochkin, Y. & Khaletskiy, Y., 2014, Turbulence control screen impact on turbofan noise spectra in far sound field, 21st International Congress on Sound and Vibration, pp 857, 2014.

[19] Salze, E., Ollivier, S., Blanc-Benon, P., Yuldashev, P., Averiyanov, M. & Khokhlova, V., 2011, Characterisation of the sound field emitted by an electric spark source in air, Forum Acusticum 2011, 27 June - 1 July, Aalborg, Denmark.

[20] Stephens, D. B., 2015, The Acoustic Environment of the NASA Glen 9- by 15-Foot Low-Speed Wind Tunnel, *21st AIAA/CEAS Aeroacoustics Conference*, No. 2015-2684.

[21] Tapken, U., Bauers, R., Neuhaus, L., Humphreys, N., Wilson, A., Stöhr, C. & Beutke, M., 2011, A New Modular Fan Rig Noise Test and Radial Mode Detection Capability, *17th AIAA/CEAS Aeroacoustics Conference*, No. 2011-2897.

[22] Wazyniak, J. A., Shaw, L. M. & Essary, J. D., 1977, Characteristics of an anechoic chamber for fan noise testing, *[NASA Technical Memorandum*, No. TM X-73555.

[23] Woodward, R. P., Wazyniak, J. A., Shaw, L. M. & MacKinnon, M. J., 1977, Effectiveness of an inlet flow turbulence control device to simulate flight noise in an anechoic chamber, *J. Acoust. Soc. Am.*,**62**.